AIAA AVIATION 2019
17 - 21 Jun 2019, Dallas, TX
AIAA-2019-3385

Effect of Varying Beam Diameter on Global Jitter of Laser Beam Passing Through Turbulent Flows

Luke Butler[1], Mitchell Lozier[2], Stanislav Gordeyev[3]
University of Notre Dame, Notre Dame, IN, 46556

The experimental studies of the global beam jitter of a collimated laser beam for different beam diameters due to the turbulent boundary layers on tunnel walls are presented. The global jitter spectra were found to be attenuated at high frequencies due to an aperture-averaging effect. Results for the jitter spectra attenuation of the streamwise jitter component qualitatively agree with a one-dimensional model, developed earlier. For the spanwise global jitter, an empirical curve fit was developed to describe amount of attenuation imposed on the beam. Various contamination effects, potentially corrupting the data, were also presented and discussed.

I. Introduction

As a laser beam passes through turbulent flow, aero-optical structures of fluctuating densities will impose optical aberration on the beam and, among other things, will cause the beam to propagate in a different direction. This is known as a beam deflection or beam jitter. For small beam diameters, Huygens principle states [1] that the beam will be deflected by amount proportional to the 2-D gradient of Optical Path length (OPL),

$$\theta_x(t) = \frac{\partial}{\partial x} OPL(x,y,t),\ \theta_y(t) = \frac{\partial}{\partial y} OPL(x,y,t),$$

as schematically shown in Figure 1. OPL, in turn, is an integral of the density field along the beam propagation,

$$OPL(x,y,t) = K_{GD} \int \rho(x,y,z,t)dz, \tag{1}$$

where K_{GD} is Gladstone-Dale constant [1]. If the convective speed is known, OPL can be reconstructed from the deflection angle signals using the Taylor frozen field hypothesis [2,3],

$$OPL(t = -U_C x) = -U_C \int_{t_o}^{t} \theta(t)dt\ .$$

Thus, by projecting a single small-aperture laser beam through turbulent flows, wavefronts can be directly measured if the convective speed is known. As wavefronts are proportional to the integrated density field, Eq (1), analysis of the time series of deflection angles is very informative way to learn about the underlying turbulent flow. This approach was successfully used to study boundary layers [1,2,4], shear layers [1,5,6] and flows around turrets [3,7,8].

[1] Graduate student, Department of Aerospace and Mech. Eng AIAA Student member.
[2] Graduate student, Department of Aerospace and Mech. Eng AIAA Student member.
[3] Associate Professor, Department of Aerospace and Mech. Eng., AIAA Associate Fellow

The main issue with this approach is that wavefronts are integrated quantities and do not provide any information about where along the laser beam the optical distortions happen. For spanwise-uniform flows, this problem can be addressed by collecting wavefronts in both wall-normal and spanwise directions [9], but it general it is a drawback of any optical technique which involves a collimated laser beam.

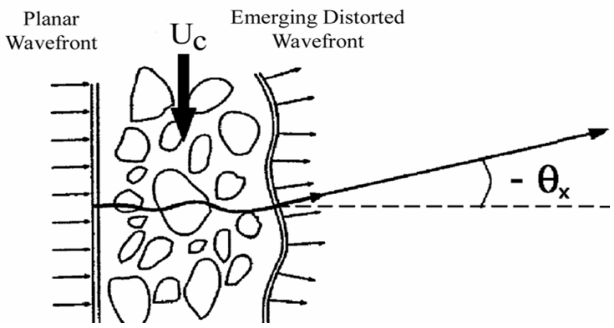

Figure 1. Beam deflection due to turbulent flow

While the source of beam jitter cannot be located along the beam, the amount of jitter depends on the beam aperture size, or to be exact on the ratio of the size of optical structures and the beam aperture. Smaller aberrating optical structures will have little effect on the global beam jitter, while aberrating optical structures on the same order as or larger than the beam aperture will have an effect on the global jitter [7]. When the beam aperture is large, compared to the typical aberrating optical structures in the flow, the contribution to the overall beam deflection from this flow is very small due to an aperture-averaging effect, which works as a low-pass filter, effectively suppressing high spatial frequencies, present in the wavefronts [7,10]. Figure 2 presents the amount of beam jitter, imposed on the laser beam by a turbulent subsonic boundary layer; the overall beam jitter for apertures, larger than several BL thicknesses, is hundred times less than for the small-size beams.

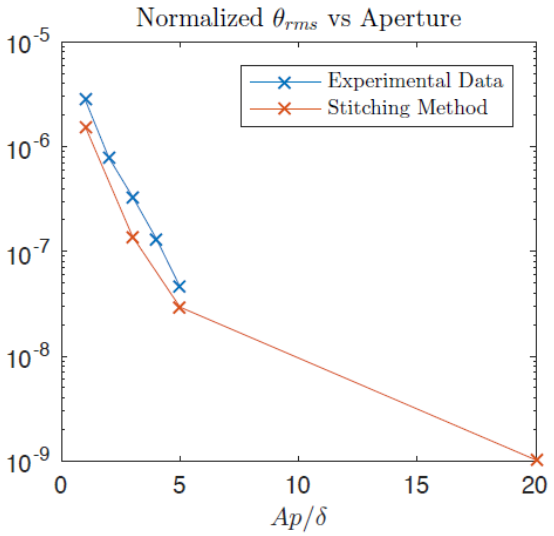

Figure 2. Normalized overall beam jitter due to a boundary layer as a function of the beam size, Ap. From [10]

While conventional Malley probes and Wavefront sensors are non-intrusive measurement techniques, capable of measuring line-integral optical path length (OPL) and an overall convective speed of the aberrating structures [2,11], the results can be corrupted by other optically aberrating flows along the laser beam, like a boundary layer on the tunnel wall, for instance. The same comment goes to Schlieren or interferometry techniques. If optical distortions of the flow of interest are dominant, compared with the optical distortions due to the boundary layer, the corrupting effects are small. However, if these optical distortions are the same order, it is very difficult to isolate the corrupting effects from the boundary layer.

To overcome this averaging-along-the-line issue, a Focused Schlieren technique [13] and Focused Laser Differential Interferometry (FLDI) [14] were developed and found to be capable of measuring optical distortions inside a compact region along the beam. Both of these techniques are intensity based, that is the optical distortions result in the intensity changes on a receiving

optical element, a digital camera for the Focused Schlieren system or a photodiode for FLDI. As laser intensity or its spatial distribution can be affected by non-ideal optical elements, these techniques require good quality optical set-ups and the careful alignment of its elements. They are also very sensitive to the vibrations of its optical elements.

Shack-Hartmann type wavefront sensors, including the Malley probe, on the other hand, record instantaneous dot displacements behind the lenslet array and reconstruct the wavefront from these dot displacements using Southwell method, for instance [15]. As the dot position is insensitive to the intensity, these sensors are much less sensitive to the beam non-uniformity, non-ideal optics or other factors which can locally affect the beam intensity. Also, effects of overall beam vibrations are relatively easy to remove from the wavefronts, allowing these sensors to collect reliable data in large industrial wind tunnels, for instance. Thus, it would be beneficial to develop a Shack-Hartmann type sensor with a focusing ability. One way to do is to utilize the aperture averaging property, discussed before, which would suppress the overall beam deflection in regions with a large beam diameter. One possible configuration is a convergent-divergent laser beam, schematically shown in Figure 3, passing through a tunnel with the boundary layers present on the wall. A collimated beam with a large diameter is focused on a point inside the tunnel. After the focusing point, beam diverges and, after passing through a second focusing lens, is forwarded to a Position Sensing Device (PSD), which measures the overall beam jitter. The total beam deflection is an integral of averaged-over-area beam deflections along the beam. Where the beam diameter is large compared to the aberrating optical structures, the contribution to the overall beam deflection is very small due to the aperture-averaging effect. Consequently, boundary-layer-related optical effects on both sides of the tunnel windows, while large in amplitude, *should not significantly contribute* to the overall beam deflection. Only the focal point region, where the beam diameter is small, has the largest effect on the total beam deflection. This results in the main contribution to the deflection of the beam occurring primarily along the portion of the beam near the focal point, where the beam has the smallest diameter,

$$\theta_x(t) = \frac{\partial OPD(x,y,t)}{\partial x} \approx K_{GD}\frac{\partial}{\partial x}\int_{-L/2}^{L/2}\rho(x,y,z,t)dz = K_{GD}L\frac{\partial}{\partial x}\left\langle \rho(x,y,z,t)\right\rangle_L$$

$$\theta_y(t) \approx K_{GD}L\frac{\partial}{\partial y}\left\langle \rho(x,y,z,t)\right\rangle_L \quad ,$$

where L is the length of the beam with the small diameter and brackets denote along-the-beam averaging. Thus, the deflection angle or beam jitter is proportional to the density gradient near the focal point.

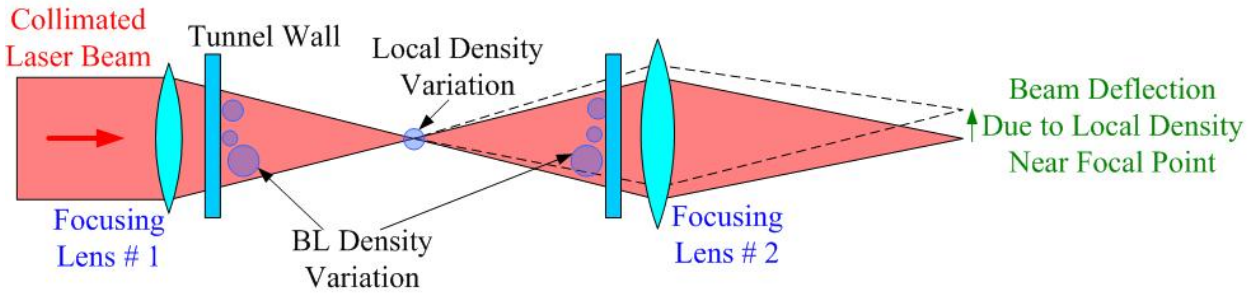

Figure 3. Conceptual schematics of convergent-divergent beam experiment

This effect has important implications in that it could potentially lead to a new way of non-intrusively measuring density fluctuations near the region of the focal point. This measurement technique could be used in hypersonic tunnels, for instance, where a number of measuring sensors are limited. Hotwires, for example, are generally too delicate for hypersonic measurements, while sonic anemometers have the disadvantage of lacking scalability when compared with a point measurement technique. In addition, both of these techniques are intrusive. Conventional Malley probes and Wavefront sensors would have significant interference from the perpendicular tunnel walls due to the line-integral method of these techniques, while yet other techniques such as PIV, PTV, DGV, LDA, and others have the disadvantage of needing to seed the flow with tracer particles.

The aperture-related analysis, provided in [7], assumed that wavefronts are one-dimensional and derived a low-pass transfer function, relating small-aperture and large-aperture jitter spectra. As real wavefronts are two-dimensional, the transfer function will be different and depend on wavefront's spatial correlations in both dimensions. In this paper, we experimentally measured jitter spectra due to a subsonic boundary layer using various beam diameters. We compared the results in the streamwise direction to the theoretical one-dimensional transfer function and also collected jitter data in the spanwise direction, which is not accounted for in the transfer function. Based on this data, we experimentally determined an empirical fit for the spanwise direction.

II. Experimental Set-Up

Experiments were performed using the 4"x4" transonic in-draft wind tunnel at the Hessert Research Laboratory at the University of Notre Dame. The wind tunnel test section has optical quality glass installed on the sides where the laser beam was transmitted through. A small-aperture, ~1mm, 532 nm YaG:Nd laser beam was expanded to a 1-inch beam using a collimator, as shown in Figure 4. Additional lenses and a variable aperture iris were used to expand or contract the beam to diameters of 0.25, 0.50, 0.75, 1.00, and 1.50 inches. After expanding or contracting the beam to a certain diameter, it was transmitted through the tunnel test section in the span-wise direction. After passing through two boundary layers on the test section walls, the beam was diverted to pass back below the tunnel using a set of mirrors and a 1.5 meter focal length lens was used to converge the beam to a point on a duo-lateral optical position sensing device (PSD). A cardboard tube and an additional iris were used in front of the PSD to reduce the amount of stray glowing laser light reaching the sensor.

The time-resolved overall beam jitter for different beam diameters and flow speeds was collected by recording the instantaneous beam positions of the focused beam on the PSD. To collect data with the smallest beam diameter, all lenses except for the last focusing lens were removed and the laser beam with a diameter of 0.04 in, or ~1mm, was transmitted through the test section. This data set will be referred as the local beam jitter, and the datasets for other beam diameters will be called global beam jitter.

The PSD was attached to a two-direction translation stage for calibration in the X (streamwise) and Y (spanwise) directions. This translation stage was itself affixed to a translation stage in the Z direction, shown in Figure 4, in order to find the exact focus location of the beam. Because the beam got slightly rotated when being directed below the tunnel using the set of

mirrors, the PSD was rotated at an angle of 12.5 degrees so that jitter caused by fluctuations in the horizontal or stream-wise direction in the test section would remain in the horizontal direction when directed onto the PSD.

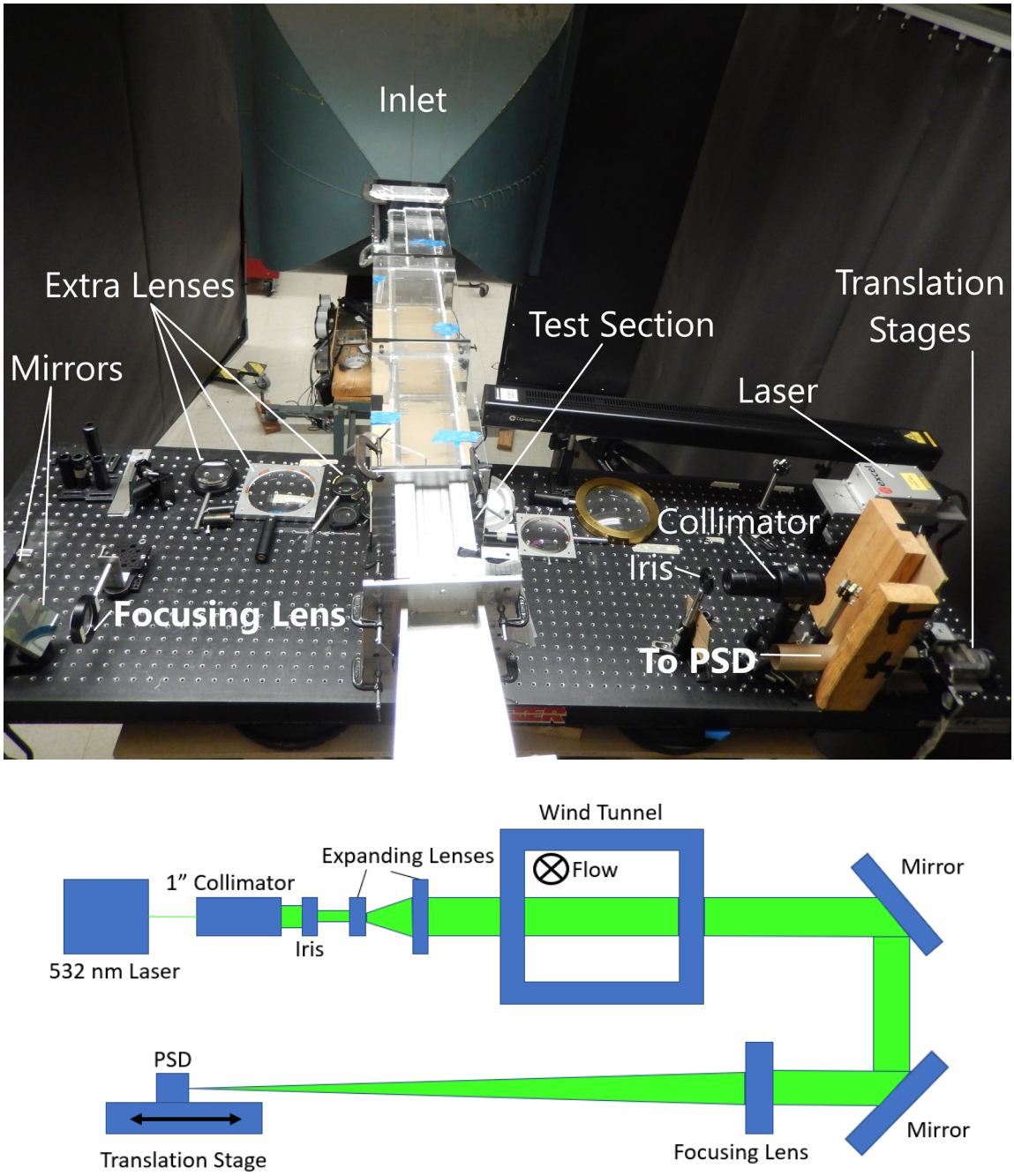

Figure 4: A picture (top) and a schematic (bottom) of the experimental set-up for variable beam diameter experiments

A variable intensity 2 Watt 532 nm Nd:YAG laser was used to ensure the intensity of the light on the PSD was sufficient across all aperture diameters. The tunnel was run at Mach numbers

of 0.4, 0.5, and 0.6, verified by a static pressure port, and the only structures in the flow affecting the beam jitter were assumed to be structures in the boundary layers created by the tunnel walls. Results for only the Mach 0.4 case are reported in this paper, as other Mach numbers provided similar results.

Beam displacements in both the horizontal and the vertical directions were recorded using a duo-lateral position sensing device (PSD) as mentioned previously. Sum and difference voltages for each direction were collected at a frequency of 150 kHz over a sampling time of 30 seconds. The difference voltages that were collected from the sensor were normalized by the sum voltages in order to eliminate any laser intensity dependent fluctuations from the data. Calibration was performed using a translation stage so that coefficients relating voltage readings to the physical beam displacement near the center of the position sensing device could be determined. The beam displacement readings from PSD, (Δx, Δy), were then divided by the focal length of the final focusing lens, f = 1.5 m, in order to find the angular displacement otherwise referred to as the jitter of the beam in both directions, (θ_x, θ_y) = (Δx, Δy)/f. The mean of the beam jitter was removed and the jitter power spectra were computed using $\left|\hat{\theta}_G(f;Ap)\right|^2$ block averaging scheme such that the final frequency resolution was 20Hz for all power spectra data. The local jitter power spectra will be denoted as $\left|\hat{\theta}(f)\right|^2$.

At the measurement location, the boundary layer thickness, δ, was 15.6 mm, giving the following values for the beam aperture to boundary thickness ratios: Ap/δ = 0.4, 0.8, 1.2, 1.6 and 2.4. The temperature in the lab remained constant at 22.6ºC throughout the experiments, and it was used to determine the free stream velocity for a known Mach number.

III. Sensitivity Analysis

There are several factors in this experiment which can negatively affect the data, and which must be mitigated in order to obtain quality data. One source of error or contamination which can have a major effect is a rotation of the PSD with respect to the X (streamwise) – Y (spanwise) coordinate system of the flow. In this experiment, the return mirrors to the right in Figure 4 (bottom) rotated the beam off of the desired coordinate system by 12.5º. This was unavoidable for this setup because the PSD and translation stage could not lie in the same plane as the collimator. The amount of rotation in the beam can be measured by covering either the upper or lower half of the beam at the tunnel, placing an extra lens between the focusing lens and the PSD so that the beam diameter is about an inch at the PSD, and measuring the angle. Figure 5 shows the effect of a beam rotated 12.5º off from the axes of the PSD. Even at this relatively small angle, there is significant contamination from the spanwise direction, causing a significant discrepancy around 1000 Hz.

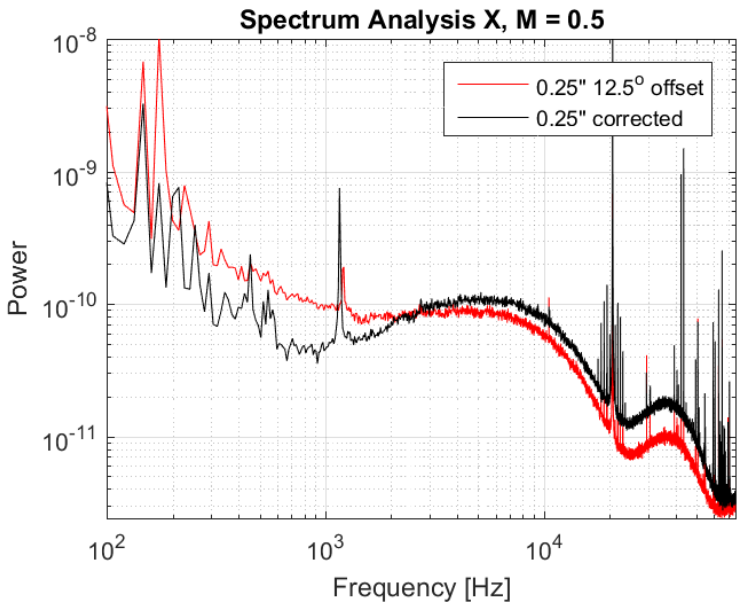

Figure 5: Effect of rotating PSD 12.5° off flow coordinates

Another source of error affecting the spectra comes from the beam being 'off focus' on PSD, when PSD is either too close or too far from the final focusing lens, resulting in a small circle rather than a focused dot on the sensor. To find this focus location, the sum voltages were measured at different distances from the focusing lens, or z locations, using a translation stage represented in Figure 4. An example of a plot used to find this focus location for a certain setup is shown in Figure 6. The noise was relatively small over the full 4" range of the translation stage, but had a greater effect when zooming in to find the exact focus, which could be found to within 0.1". Any possible lensing effect due to Mach numbers up to 0.6 were not found to have any discernable effect on the focus location, and if there is an effect, it is smaller than this 0.1" range of precision.

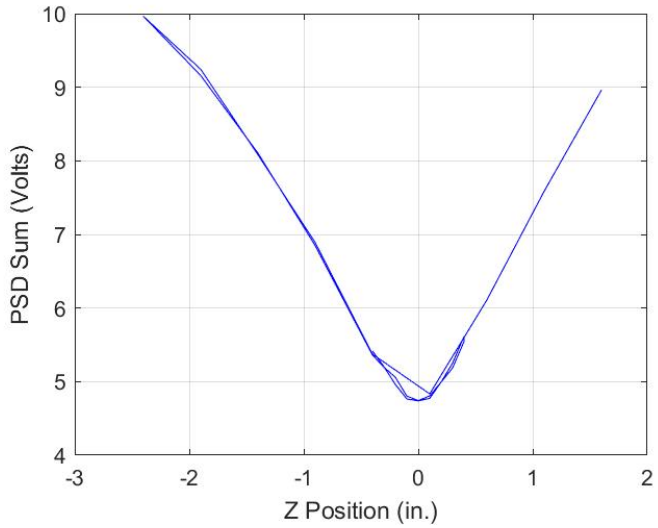

Figure 6: Voltage X-sums on PSD for 1" beam as a function of the PSD location relative to the beam focal point

A plot showing the effect on the spectra of translating the PSD to various z-locations for a 1" aperture beam is shown in Figure 7. This plot shows that an off-focus PSD does not affect the spectrum below 5 kHz, but has a significant effect on the spectrum above 5 kHz. Figure 8 shows the same corrupting effect for a 0.25" beam, but to a much lesser extent because of the shallower angle for a smaller beam resulting in smaller changes to beam size for the same amount of translation in the z direction, when compared with a larger aperture beam.

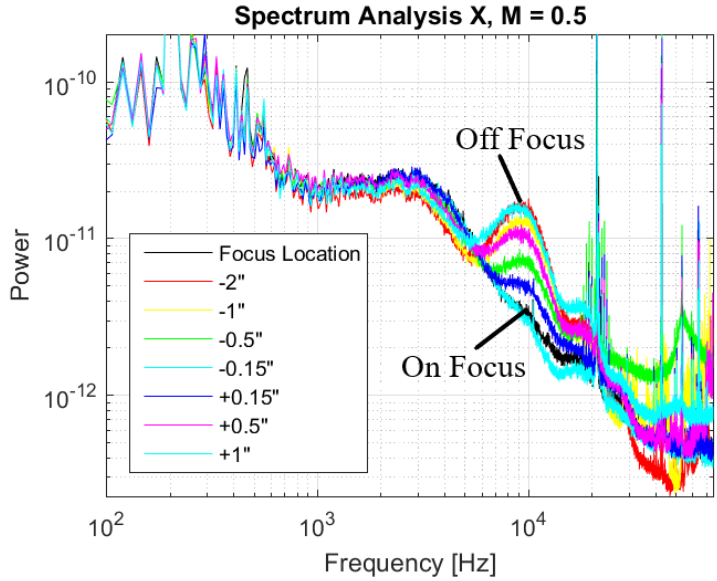

Figure 7: Effect of translating PSD in z-direction away from the focal point on the x-jitter spectrum for 1" aperture beam

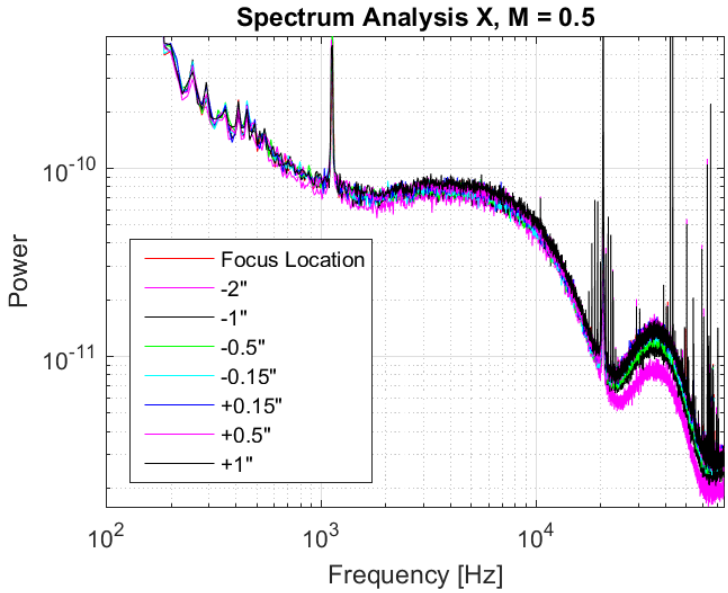

Figure 8: Effect of translating PSD in z-direction away from the focal point on the x-jitter spectrum for 0.25" aperture beam

Another source of error which can have an effect on the data is inadequate laser intensity. As shown by Figure 9, if the laser intensity is too low, there will be too much noise to get a good signal. Another interesting effect is that if the laser intensity is too high, it will also affect the spectrum shape at high frequencies due to possible saturation of the PSD.

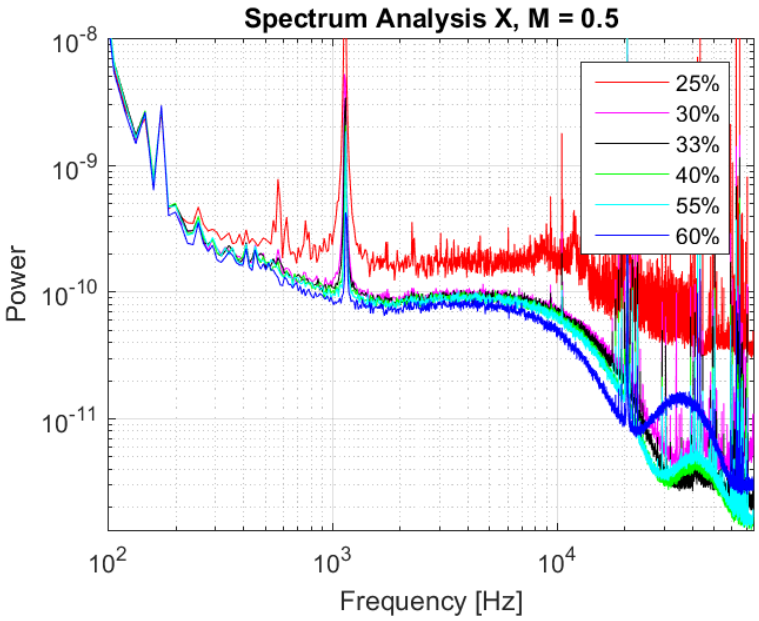

Figure 9: Effect of laser intensity on a global x-jitter spectrum imposed on 0.25” aperture beam for M = 0.5

To eliminate vibrational contamination from vibrating optical elements, the breadboard was placed on rubber tires. Also, we ensured nothing on the setup was physically touching the wind tunnel in order to reduce the effect of vibrations.

Another possible source of significant error is the effect of spherical aberrations due to the use of common spherical lenses with a focal length of less than roughly ten times the beam diameter. This prevents the beam from focusing to a point because there are different foci for different radii in the lens, which creates haloing, among other effects. If this effect is significant enough, it can lead to a completely nonsensical power spectrum. In order to avoid this, lenses of sufficient focal length for the beam diameter were used in the experiment. The lenses used to expand to the largest beam of 1.5” were just on the edge of this requirement, adding small aspherical aberrations, although they were not significant enough to result in corrupted data.

A final potentially significant source of error is electronic noise. While this cannot be eliminated completely, it can be mitigated through the use of shielding, increasing the distance from sources of potential contamination, finding electronic equipment and sensors with less noise through trial and error, and taking multiple samples for each test case until a good dataset is collected. While this can help reducing noise enough to obtain a meaningful signal, narrow spikes are likely to be present in the data, which could only be removed if the data were post-processed.

IV. Streamwise (X) Results

A plot of the power spectra of the beam jitter at different beam apertures for Mach 0.4 flow is shown in Figure 10. The spectrum for the smallest beam corresponds to the local beam jitter, since there is no attenuation due to beam size for this beam. The shape of the spectrum agrees with similar measurements of the local beam jitter in turbulent boundary layers [2]. As the beam aperture gets larger, the attenuation of the beam jitter spectra begins at higher frequencies, and the lower bound of attenuated frequencies shifts to the smaller frequencies. This behavior is expected because the effect of the larger beam apertures should be to spatially average beam jitter from small-scale structures in the boundary layer that correspond to higher frequencies in the power spectra.

There are a few factors in this plot not due to aero-optical effects that should be explained. The higher amplitude noise at frequencies below 1 kHz is mostly due to mechanical vibrations that are present when the wind tunnel is in operation, and the power spectra for different apertures in this range tend to converge. At the higher frequency end, these plots tend to reach a noise floor, which varies slightly for each measurement set. This noise floor due to the sensor/electronics noise masks any of the signal below it. In addition, all of the sharp spikes near 20 kHz and above 30 kHz in the spectra are due to electronics/sensor noise. Both the noise floor and the mechanical vibrations are left in Figure 10 and 12, but are removed for the processed data in Figures 11, 13, and 14.

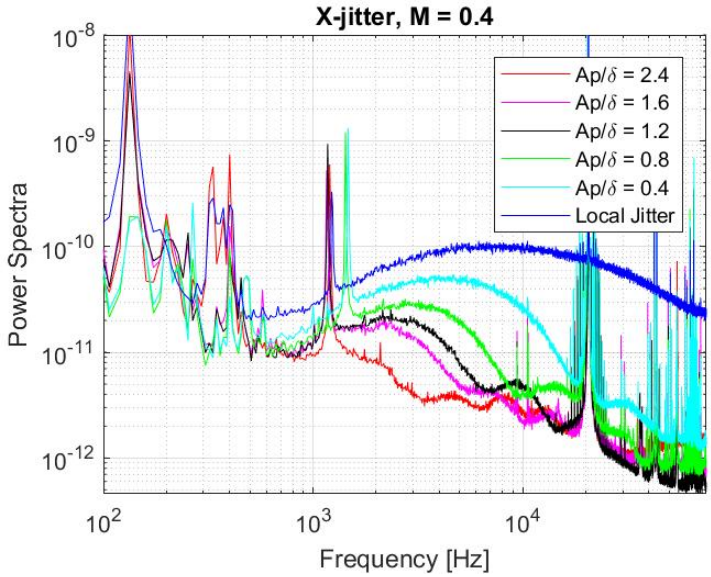

Figure 10: Power spectra of global beam jitter for different beam apertures in the streamwise direction at a free stream Mach number of 0.4

In [7] it has been shown that the theoretical ratio of global jitter spectral amplitude to local jitter spectral amplitude for one-dimensional periodic wavefront in the streamwise direction can be expressed through the aperture dependent transfer function, called $G_{Stream}(z)$,

$$G_{Stream}(z) = \frac{|\theta_G(f;Ap)|}{|\theta(f)|} = 2\left[\sin(\pi z) - \pi z \cos(\pi z)\right] / (\pi z)^3 \qquad (2)$$

where the parameter $z = {}^{Ap}/_{\Lambda}$ is the aperture diameter divided by the spatial wavelength. For convective structures traveling at the same speed of U_c, the spatial wavelength is defined as $\Lambda = U_c/f$, where of convective velocity U_c is approximately 0.82 of U_∞ for subsonic boundary layers [2]. Z-parameter is related to the aperture-based Strouhal number as:

$$z = \frac{Ap}{\Lambda} = \frac{Ap}{U_c / f} = \frac{Ap \cdot f}{U_c} = \frac{Ap \cdot f}{U_\infty} \frac{U_\infty}{U_c} = \frac{1}{0.82} \frac{Ap \cdot f}{U_\infty} = 1.22 St_{Ap} \ .$$

Figure 11 shows the ratios of the global jitter power spectra to the local jitter power spectra for various beam diameters, expressed as Ap/δ-parameter as a function of z (or equivalently, as a function of St_{Ap}). The model in Eq. (2) predicts that all spectra ratios should collapse onto a single curve. Indeed, all spectral ratios exhibit a collapse for z < 1 and collapse fairly close to each other for higher values of z, possibly due to noise interference having more of an effect as the signals get weaker and approach the noise floor. For all tested beam diameters, the ratios monotonically decrease for all z < 1. When z > 0.8, which corresponds to $St_{Ap} > 0.65$, the power spectra ratios are less than 0.1, indicating that due to the aperture-averaged effect, amount of spectral power of the global jitter at higher-frequency range is suppressed by more than one order of magnitude. All spectral ratios exhibit a small secondary peak between z = 1 and 2.5, and even smaller tertiary peak above z = 2.5.

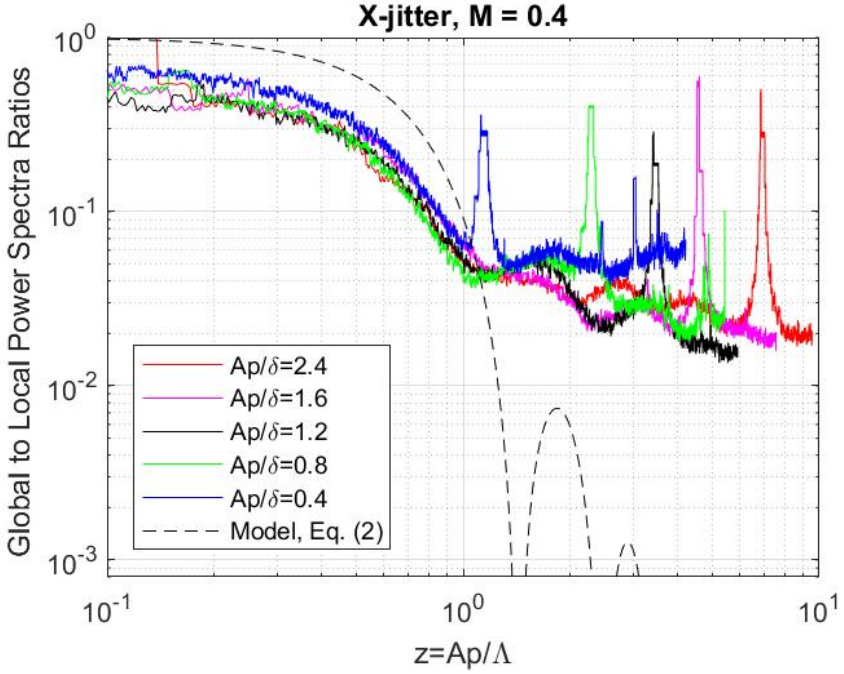

Figure 11: Ratios of global to local beam jitter power spectra for different beam aperture sizes in the stream-wise direction, processed with a smoothing algorithm to reduce noise, at a free stream Mach number of 0.4. The squared G-function is also presented a s a dashed line for comparison

The square of the aperture dependent transfer function from Eq (2) is also plotted in Figure 11 for comparison. The model correctly describes a qualitative behavior of the experimentally-observed power spectra ratios, including a monotonic decrease for small z < 1.5, and the presence of the secondary and the tertiary peaks between z= 1.5 and 2.5 and between z = 2.5 and 3.5,

respectively. However, the model-predicted attenuations are much stronger than the experimentally-observed ones. One reason for the amplitude mismatch is that the model was developed for one-dimensional wavefronts, and therefore implying a spanwise uniform wavefronts. The actual wavefronts are highly two-dimensional, contributing to larger values of the global jitter.

These experimental results demonstrate that indeed the corrupting effects due to the tunnel wall boundary layers on the global jitter can be suppressed if the aperture of the beam passing through the boundary layer is large enough. For instance, as discussed earlier, in order to achieve an attenuation of more than an order of magnitude, z should be larger than one, which corresponds to $St_{\mathrm{Ap}} > 0.65$. Recalling the definition of Shrouhal number, $St_{Ap} = \frac{Ap \cdot f}{U_\infty}$, this implies that the boundary-layer related effect on the global jitter spectrum will be small for frequencies $f > 0.65 \frac{U_\infty}{Ap}$.

These results can be used to help determining the size of beam needed to effectively eliminate jitter effects from the optical distortion from the boundary layers so that the flow features of interest at the focus location will be more easily recognizable when analyzing the power spectra. The end goal of the work is to develop a focused version of the Malley probe that will utilize the effect of spatial averaging to attenuate the effect of the tunnel wall boundary layers on beam jitter, while still being sensitive to features within the free stream of the test section near the focal point.

V. Spanwise (Y) Results

Figure 12 presents the deflection angle power spectra in the spanwise (vertical) direction. The low frequency spectra are mostly due to mechanical vibration, while the leveling off at the higher frequencies is due to the spectra dropping below the noise floor. The spikes are due to electronic noise. There still appears to be a significant attenuation in the global jitter spectra compared to the local jitter spectrum for frequencies larger than 1 kHz or so. The trend is not monotonic as for Ap/δ = 1.6 and 2.4, the spectra are leveling off above 4 kHz, while for other beam diameters, the leveling off occurs are higher frequencies above 10 kHz. The attenuation seems to be dependent of Ap/δ-ratio. The largest attenuation is achieved for Ap/δ = 1.2.

The theoretical model in Eq. (2) works only for the streamwise direction, as it links the structure streamwise size to its corresponding frequency in the spectra via the constant convective speed assumption. Therefore, it should fail when applied to the spanwise direction. Figure 13 shows the spanwise data processed in the same manner as the streamwise data in Figure 11, where frequency is converted to the aperture-dependent z parameter, and the global jitter power spectrum for each aperture size was divided by the local jitter power spectrum. As observed, these power ratios do not collapse into a single curve as the streamwise ratios do.

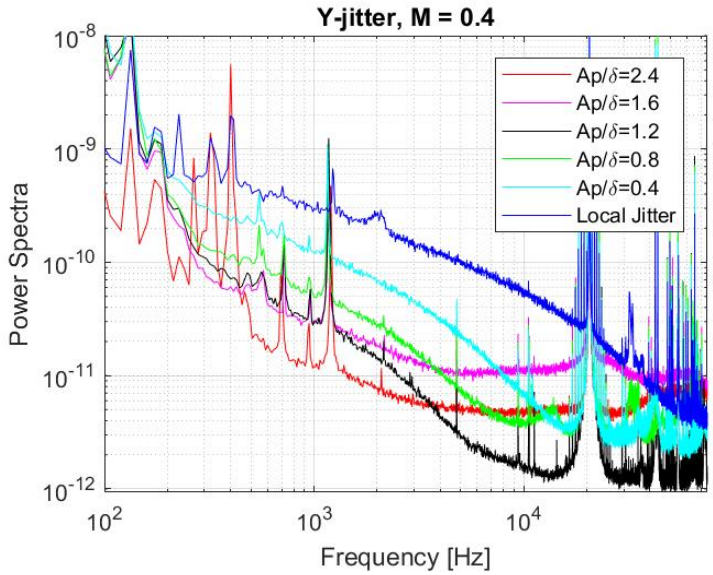

Figure 12: Power spectra of global beam jitter for different beam apertures in the spanwise direction at a free stream Mach number of 0.4

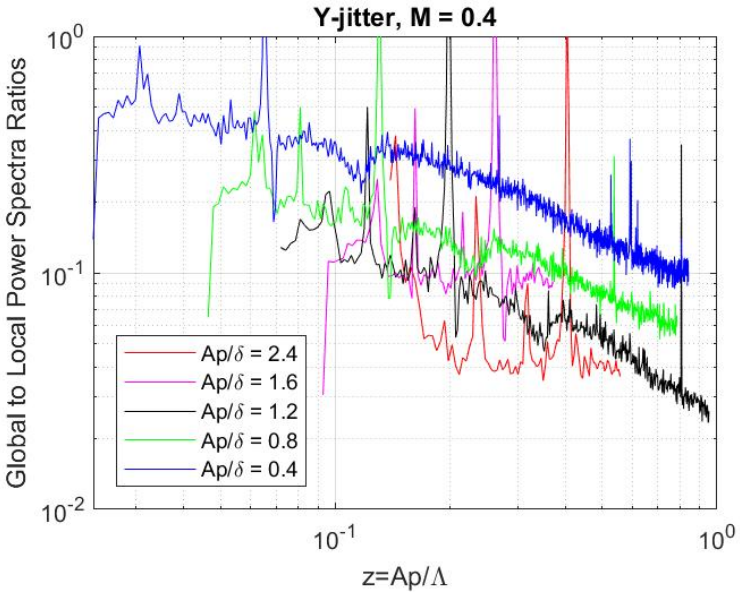

Figure 13: Ratios of global to local beam jitter power spectra for different beam aperture sizes in the spanwise direction at a free stream Mach number of 0.4

By trial and error, it was discovered that when each power spectrum ratio is multiplied by the corresponding aperture size, the ratio results tend to collapse onto a single curve, as shown in Figure 14. Using these results, an empirical curve fit was developed to approximate the collapsed curve in Figure 14,

$$G_{Span} = \frac{\left|\theta_G(f;Ap)\right|}{\left|\theta(f)\right|} = 0.125\exp\left[-1.4\left\{\log(z+1)\right\}^{1/2}\right] \tag{3}$$

This empirical fit can be used to predict the global beam jitter spectrum based on the local beam jitter spectrum and a given aperture size. Note that this empirical fit is valid only for subsonic boundary layers and circular laser beams.

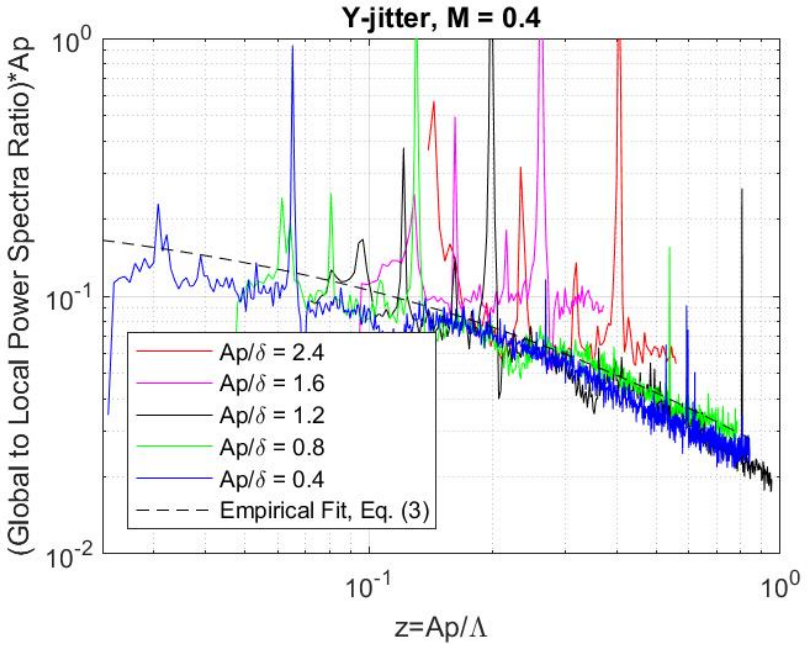

Figure 14: Ratio of global to local spanwise beam jitter multiplied by each aperture at a free stream Mach number of 0.4 compared to the square of the new aperture dependent exponential equation G_{span}

Future studies will involve using a converging-diverging beam to make point measurements both inside and outside the boundary layer in order to demonstrate the ability to infer information about the density field at different spatial points. A second convergent-divergent beam will also be added to provide means to measure the convective speed of optical aberration near the focal points. Future work will also utilize these results to investigate and develop a model of the effects of various optical structures along a convergent-divergent beam on the overall resulted beam jitter and eventually develop an working sensor, a Focused version of the Malley probe, capable of measuring optical distortions inside a compact region near the focal point.

VI. Conclusions

The experimental studies of the global beam jitter imposed on a laser beam with different diameter by compressible subsonic turbulent boundary layers are presented. The time-resolved global beam jitter was measured using a single position sensing device. Measurements of the global bean jitter on the streamwise and the spanwise direction were performed and the analysis of power spectra were conducted. Various sources of error, effecting the quality of the measurements were investigated and possible ways to eliminate them are provided. It was found that for both components of the jitter, the aperture averaging effect resulted in a suppression of the beam jitter spectra at high frequencies. For the streamwise component of jitter, larger beam

apertures lead to larger suppression. For both components of the jitter, the ratios of global to local beam jitter power spectra were also studied. For the streamwise component of jitter, the ratios were found to approximately collapse onto a single curve, when plotted vs a ratio of the beam diameter to the structure size. The results were also compared with an analytical model, developed earlier for the one-dimensional wavefronts, and a qualitative agreement between the results and the model was observed. The model was found to overpredict the amount of the suppression in the streamwise jitter spectra. For the spanwise component of jitter, the spectra ratio were found to collapse vs the aperture-to-size ratio, if the ratio is multiplied by the aperture size, and the empirical curve fit was provided.

These results will be used to develop a focused version of the Malley probe with convergent-divergent beams, capable of measuring the deflection angles and the related convective speeds inside a compact region near a focal point, while minimizing the corrupting effects from turbulent boundary layers present on the tunnel walls. Future work will also include developing a model for the convergent-divergent beams to better interpret the Focused Malley probe results.

References

[1] S. Gordeyev, E.J. Jumper, “Physics and Measurement of Aero-Optical Effects: Past and Present,” Annual Review of Fluid Mechanics, **49**, pp. 419–441, 2017

[2] S. Gordeyev, A. E. Smith, J.A. Cress and E.J. Jumper, “Experimental studies of aero-optical properties of subsonic turbulent boundary layers," *Journal of Fluid Mechanics*, **740**, pp. 214-253, 2014.

[3] S. Gordeyev, T. Hayden and E. Jumper, "Aero-Optical and Flow Measurements Over a Flat-Windowed Turret", *AIAA Journal*, **45**(*2*), pp. 347-357, 2007.

[4] S. Gordeyev, J.A. Cress, A Smith and E.J. Jumper, " Aero-optical measurements in a subsonic, turbulent boundary layer with non-adiabatic walls", Physics of Fluids, 27, 045110, 2015.

[5] Malley M, Sutton GW, Kincheloe N. 1992. Beam-jitter measurements of turbulent aero optical path differences. Appl. Opt. 31:4440–43.

[6] Fitzgerald, E., and Jumper, E. (2004). The optical distortion mechanism in a nearly incompressible free shear layer. Journal of Fluid Mechanics, 512, 153-189.

[7] N. De Lucca, S. Gordeyev, and E. Jumper, "The Study of Aero-Optical and Mechanical Jitter for Flat-Windowed Turrets", AIAA Paper, 2012-0623.

[8] B. Vukasinovic, A. Glezer, S. Gordeyev, E. Jumper and V. Kibens, "Fluidic Control of a Turret Wake: Aerodynamic and Aero-Optical Effects", AIAA Journal, Vol. 48,No, 8, pp. 1686-1699, 2010.

[9] J. Sontag and S. Gordeyev, "Non-intrusive Velocity and Density Measurements in Subsonic Turbulent Boundary Layer ", AIAA Paper 2015-3247, 2015.

[10] M.R. Kemnetz and S. Gordeyev, “Multiple aperture approach to wavefront prediction for adaptive-optic applications,” AIAA Paper 2017-1344, 2017.

[11] A.E. Smith, S. Gordeyev, H. Ahmed, A. Ahmed, D.J. Wittich III and M. Paul, " Shack-Hartmann Wavefront Measurements of Supersonic Turbulent Boundary Layers in the TGF ", AIAA Paper 2014-2493, 2014.

[12] S. Gordeyev and T.J. Juliano, "Optical Measurements of Transitional Events in a Mach-6 Boundary Layer", AIAA Journal, Vol. 55(11), pp. 3629-3639, 2017.

[13] L.M. Weinstein,"Large-field high-brightness focusing schlieren system", AIAA Journal, 31(7), pp. 1250-1255, 1993.
[14] G.S. Settles, M. R. Fulghum, "The Focusing Laser Differential Interferometer, an Instrument for Localized Turbulence Measurements in Refractive Flows", Journal of Fluids Engineering, 138(10), 2016
[15] W. H. Southwell, "Wave-front estimation from wave-front slope measurements," J. Opt. Soc. Am. 70(8), pp. 998–1006, 1980